Pergamon

www.elsevier.nl/locate/asr

PII: S0273-1177(99)00692-4

Adv. Space Res. Vol. 24, No. 9, pp 1105-1114, 1999
© 1999 COSPAR. Published by Elsevier Science Ltd. All rights reserved
Printed in Great Britain
0273-1177/99 $20.00 + 0.00

THE PANORAMIC CAMERA OF THE ROSETTA MISSION: PERFORMANCES OF PROTOTYPE 3D MICROCAMERAS

S. Beauvivre, P. Lamy, T. Nguyen-Trong, and J.-L. Reynaud

Laboratoire d'Astronomie Spatiale, BP 8, 13376 Marseille Cedex 12, France

ABSTRACT

We present the evaluation of the performances of microcameras prototypes manufactured in 3D packaging technology developed for the panoramic camera of the lander for the ROSETTA cometary mission. Two different prototypes were tested, one manufactured by Alcatel and the other by CSEM. A specific laboratory setup with cooling capabilities was implemented to perform electrical, mechanical and photometric tests in the temperature range –90°C to +20°C. Our results show that the photometric performances are nominal and do not change in this temperature range. The reduced size of the camera, associated with its operating mode, leads to a transient thermal behaviour that does not affect the cameras properties when operated at temperatures below –55°C. We show that this kind of miniature camera is suitable to deep space missions like ROSETTA, provided specific cares are taken in the electrical and mechanical designs. © 1999 COSPAR. Published by Elsevier Science Ltd.

INTRODUCTION

The panoramic camera is part of the in-situ imaging system for the Surface Science Package (EuroLander) of the European Space Agency (ESA) ROSETTA mission to comet 46P/Wirtanen. The early systems, ISIS for Champollion and ROLIS for RoLand (Lamy *et al.*, 1998), have now been combined into the ÇIVA experiment for the EuroLander. The panoramic camera is a lightweight imaging system designed to characterise the cometary surface near the landing site, from anchoring legs at spatial scales not achievable by the orbiter cameras, to the local horizon. It is composed of seven miniaturised identical cameras incorporating a 1024×1024 pixels, frame transfer CCD and wide-angle optics having a field-of-view of 70°. Six of them are equally spaced by 60° to record the full panorama without any mechanical rotation. The seventh camera is co-aligned with one of the above to offer stereoscopic capability in one of the six fields-of-views. The camera heads with associated electronics are integrated in a single module using the technology of three-dimensional packaging of electronic components resulting in highly compact, extremely lightweight units. The operating mode will consist in taking first a sequence of images in order to optimise the integration time so that the dynamic of the scene will match that of the cameras and then the scientific images.

These camera heads, which result from very recent developments of packaging technology (Larcombe *et al.*, 1995), are the most important and critical parts of the experiment. They must survive a long cruise in interplanetary space and operate in the very hostile environment of a cometary surface where temperatures will vary from –110°C to –50°C. Power dissipation in the heads is also of concern as the internal temperature may rise as images are being taken resulting in varying performances. It was therefore felt necessary to initiate research and technology programs aimed at validating this technology for space experiments and to verify its performances in the above conditions. A first program led by the Centre National d'Etudes Spatiales (CNES) and our laboratory resulted in the realisation of two prototypes manufactured by Alcatel Space Industries (France). A second, independent program, led by ESA, provided a different prototype (Josset *et al.*, 1997) produced by the Centre Suisse d'Electronique et de Microtechnique (CSEM). We report below the results of extended functional and opto-electrical tests of the second Alcatel prototype and the CSEM prototype.

DESCRIPTION OF THE PROTOTYPE MICROCAMERAS

The two prototypes were manufactured in MultiChip Module - Vertical (MCM-V) technology (Val and Leroy, 1991); their main characteristics are presented in Table 1. They both incorporate a frame transfer CCD array of 1024×1024 pixels:

- for the Alcatel prototype, a Thomson THX7887A chip whose image zone is divided into four areas, each one having its own readout amplifier and converter;
- for the CSEM prototype, a Thomson THX7888A chip with a single sensitive area.

In both cases, the bare chip was sandwiched between two glass plates and this device was deposited on the 3D electronic package. Figure 1 shows the Alcatel prototype with its titanium plate insuring the mechanical interface and the flex cable to the external connector. The rather thick (3 mm) front glass plate insures the flatness of the CCD. Figure 2 presents the CSEM prototype with its associated optics mounted on an aluminium stirrup. The electronic package is maintained in place by a spring. This design offers minimum thermal contact and isolates the electronic part; as a consequence, this prototype could not be cooled in vacuum conditions to avoid a potentially damaging increase of the internal temperature. The two cameras deliver a 10 bits digital output at 10 Mbits/s. In addition, the CSEM prototype offers an output at 57.6 kbits/s with 8 bits per pixel. Both include a correlated double sampling (CDS) system to remove reset noise, numerically in the Alcatel prototype and in an anolog way in the CSEM prototype.

Table 1. Characteristics of the two Prototype Microcameras

Parameter	Alcatel prototype	CSEM prototype
CCD array	THX7887A	THX7888A
Dimensions	35×25×12 mm	35×21×14.5 mm
Volume	10.5 cm^3	10.6 cm^3
Mass of the head	21 g	26 g
Power supplies lines	4	6
Power consumption	2.2 W	2.8 W
Max. output frequency	1 Mpixels/s	1 Mpixels/s
Coding range	10 bits	10 bits
CDS	digital	analog
Integration time	0-65535 ms	0-650 ms
Transfer time	1.67 ms	13.5 ms
Readout time	1 s	1 s
Antiblooming	active	non-used
Electrical protocol	non-standard	RS422
Number of video chain	4	1
Reference pixels and lines	yes	no
Internal memory	no	yes
Internal temperature probe	yes	no

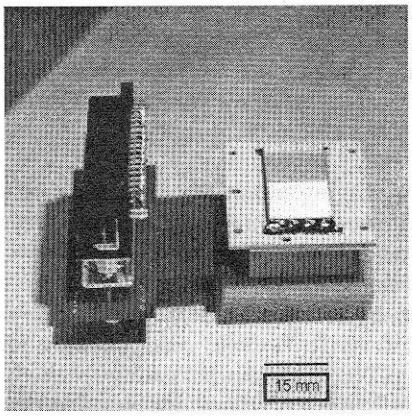

Fig. 1. *Alcatel prototype.*

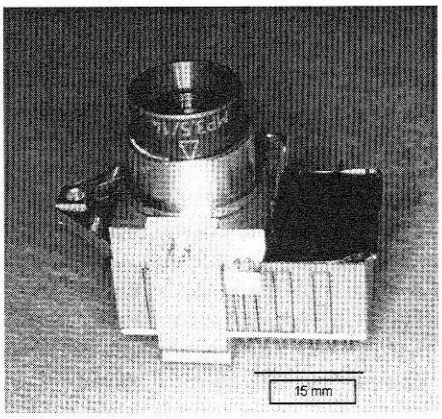

Fig. 2. *CSEM prototype.*

TEST APPARATUS AND OPERATIONS

Tests conditions of an integrated microcamera are very specific since the only available signal is its digital output. Other internal signals, usually available in a standard camera and useful to characterise the electronic chain, cannot be accessed. A test system has been realised for vacuum measurements of the Alcatel prototype, in the temperature range –150°C to +20°C, with a solar spectra uniform illumination whose intensity can be controlled. It is composed of a cryorefrigerator which cools a finger thermally connected to the microcamera, this setting being located in a vacuum chamber. The light source is composed of a main integrating sphere which is itself illuminated by a satellite sphere. A variable diaphragm and a filter mount are placed between the two spheres in order to control the radiance and the colour of the illuminating beam (Figure 3). A first temperature probe inside the Alcatel cube records its internal temperature. Another one gives the external temperature in the vacuum chamber.

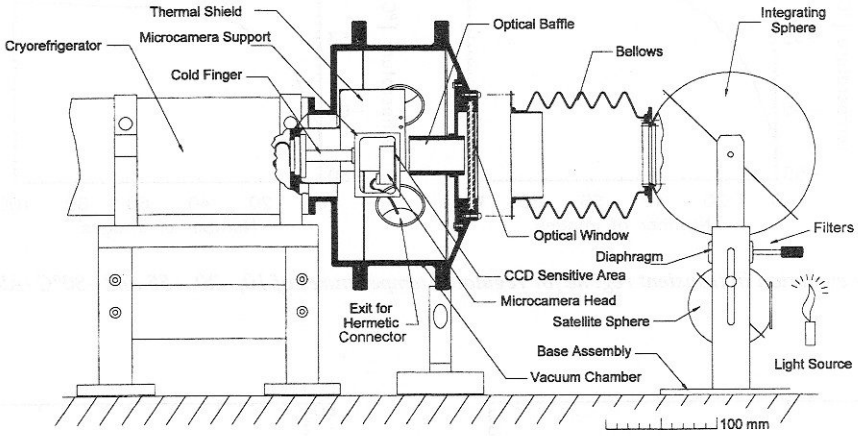

Fig. 3. *Opto-mechanical system.*

The tests are intended to characterise the operation (power consumption, analog to digital conversion) and the performances (dark current, linearity, conversion factor and noise) of the two prototypes (Beauvivre, 1999). In the case of the CSEM prototype, they were limited to room temperature and normal pressure conditions for reasons explained in the above section. In the case of the Alcatel prototype, they were performed in vacuum at different temperatures, either in a stationary mode (stabilised temperatures) or in a transient temperature mode. In this latter situation, the camera is switched on at a given temperature (the internal and external temperatures are equal) and a large number of images is taken continuously. Figure 4 presents the internal temperature as a function of the number of images for given external temperatures. It shows that the internal temperature increases substantially during the first 20 images and then stabilises after 40-60 images. Thus, for an external temperature of 10°C, the internal temperature reaches 27°C after 40 images. The difference between external and internal temperature obtained after 100 images increases with decreasing temperatures, going from about 15°C at +20°C to about 29°C at –90°C. This is due to the conjunction of two phenomena: an increase of power consumption when the temperature decreases and a decrease of the thermal conductivity of the titanium plate (8.5 W/m/K at +27°C to 6 W/m/K at –120°C).

RESULTS OF THE TESTS

Dark Current

Figure 5 present the average dark current of a line (256 pixels for a zone), expressed in digital number (DN), as a function of the line number for the first zone of the Alcatel prototype. The electronic offset being removed in this case, the dark current of the first line corresponds to charges generated during the integration time. The difference of signals between the first and the last lines results of the combined effect of thermal generation of charges during the readout process (one second) and losses due to transfer inefficiency. Figure 6 presents the mean dark current of the array of the CSEM prototype. For the first line level, the electronic offset adds to the dark current during the

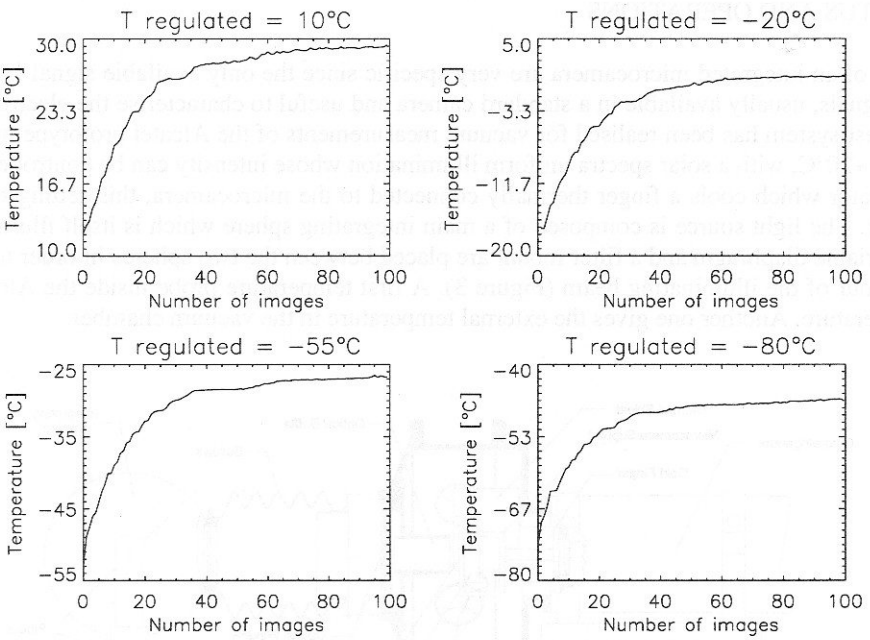

Fig. 4. *Temperature evolution in transient regime for regulated temperatures of 10, –20, –55 and –80°C (Alcatel prototype).*

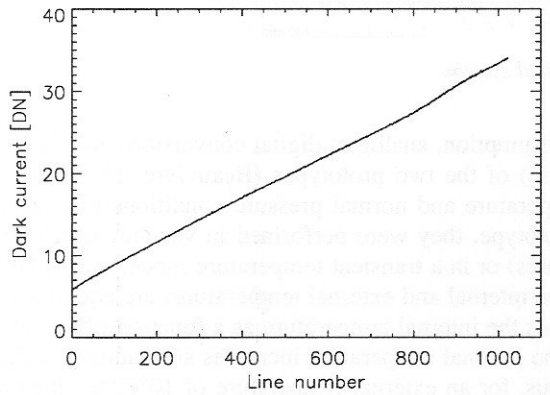

Fig. 5. *Mean dark current (offset corrected) of each line of the first zone of the array for an integration time of 100 ms at 36°C (Alcatel prototype).*

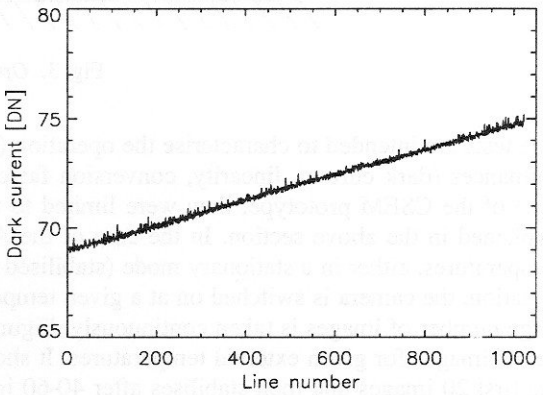

Fig. 6. *Mean dark current of each line of the array for an integration time of 550 ms (CSEM prototype).*

integration time. Figure 7 illustrates the variation of the dark current as a function of external temperature for the Alcatel prototype: the semi-log plot clearly reveals that it follows the theoretical exponential law. In transient temperature conditions, the evolution of the dark current, as a function of the number of images, is represented Figure 8. The curves show that this evolution is important at +20°C, since the dark current doubles after about 50 images. At 0°C, this phenomenon is attenuated (+50% after 50 images) and is no longer present at –55°C.

Conversion Factor and Noise

The conversion factor is defined as the number of electrons per digital number. It represents the coefficient between the input signal and the digitised output signal. Figure 9 presents the histogram of the values of the conver-

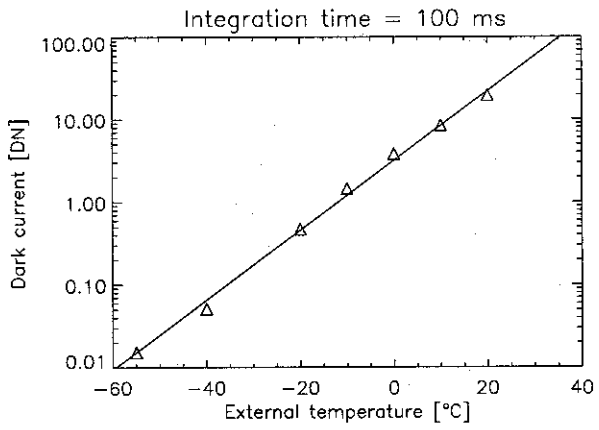

Fig. 7. *Mean dark current (offset corrected) as a function of external temperature (Alcatel prototype).*

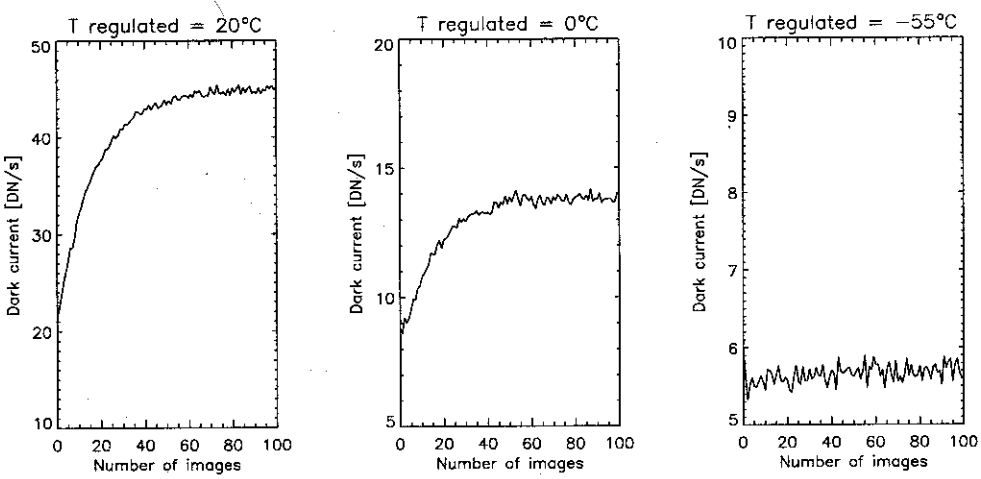

Fig. 8. *Dark current as a function of the number of images for regulated temperatures of 20, 0 and –55°C (Alcatel prototype).*

sion factor, obtained over the array of the Alcatel prototype. It shows that the conversion factor follows a quasi-gaussian distribution centred at about 125 e^-/DN. This implies that the conversion factor differs from one pixel to another. Figure 10 shows the values of the conversion factor, determined with the photon transfer technique (Janesick *et al.*, 1987), as a function of temperature for the Alcatel prototype: it remains constant over the range –90°C to +20°C.

The measured noise, which comprises all noise sources affecting the video signal, is composed of the CCD readout noise and the noise of the electronic chain, the dominant noise being introduced by the analog to digital conversion. The results obtained at different temperatures for the Alcatel prototype (Figure 11), show that this noise presents the expected value and that it does not change in the temperature range –90°C to +20°C.

Linearity

Our measurements indicate that deviation from linearity is less than 1% for both prototypes (Figure 12). In the CSEM case, the saturation level is obtained below the limit of the A/D converter indicating a non-optimal operation. On the contrary, the saturation of the CCD of the Alcatel prototype is reached at the upper limit of the 10 bits A/D converter. The CCDs have a built-in antiblooming device controlled by a gate determining the saturation level; correct biasing of this gate is required to tune the dynamic range to that of the converter.

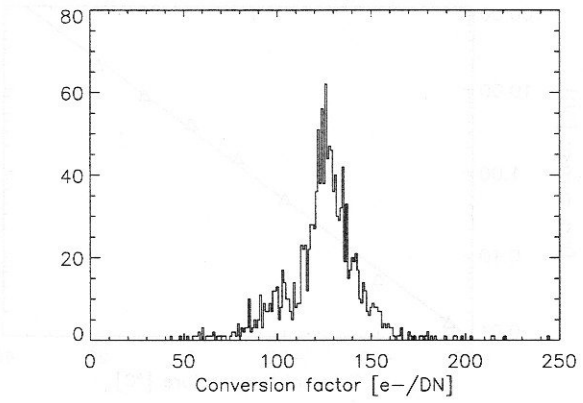

Fig. 9. *Histogram of the values of the conversion factor obtained over the array at 0°C (Alcatel prototype).*

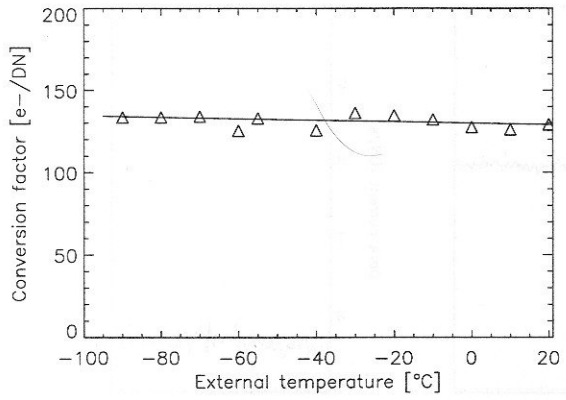

Fig. 10. *Conversion factor as a function of external temperature (Alcatel prototype).*

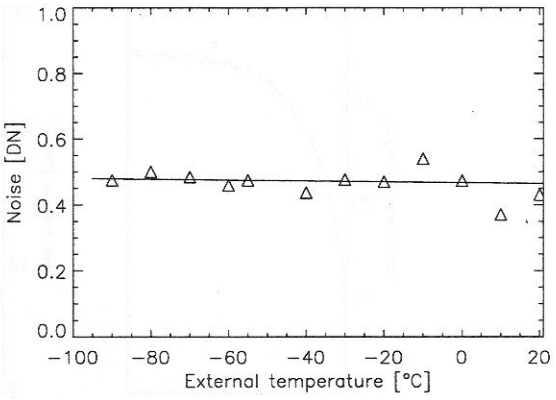

Fig. 11. *Noise as a function of external temperature (Alcatel prototype).*

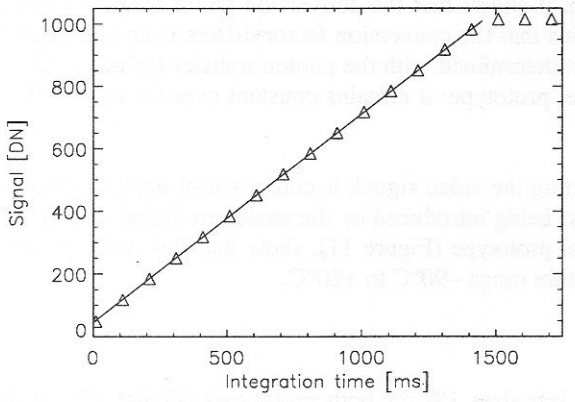

(a)

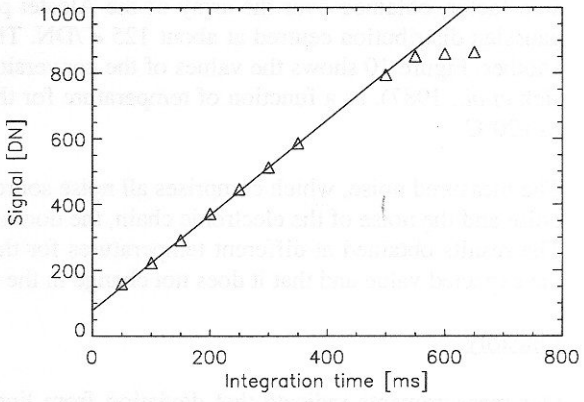

(b)

Fig. 12. *Linearity curves as a function of integration time for (a) Alcatel prototype and (b) CSEM prototype.*

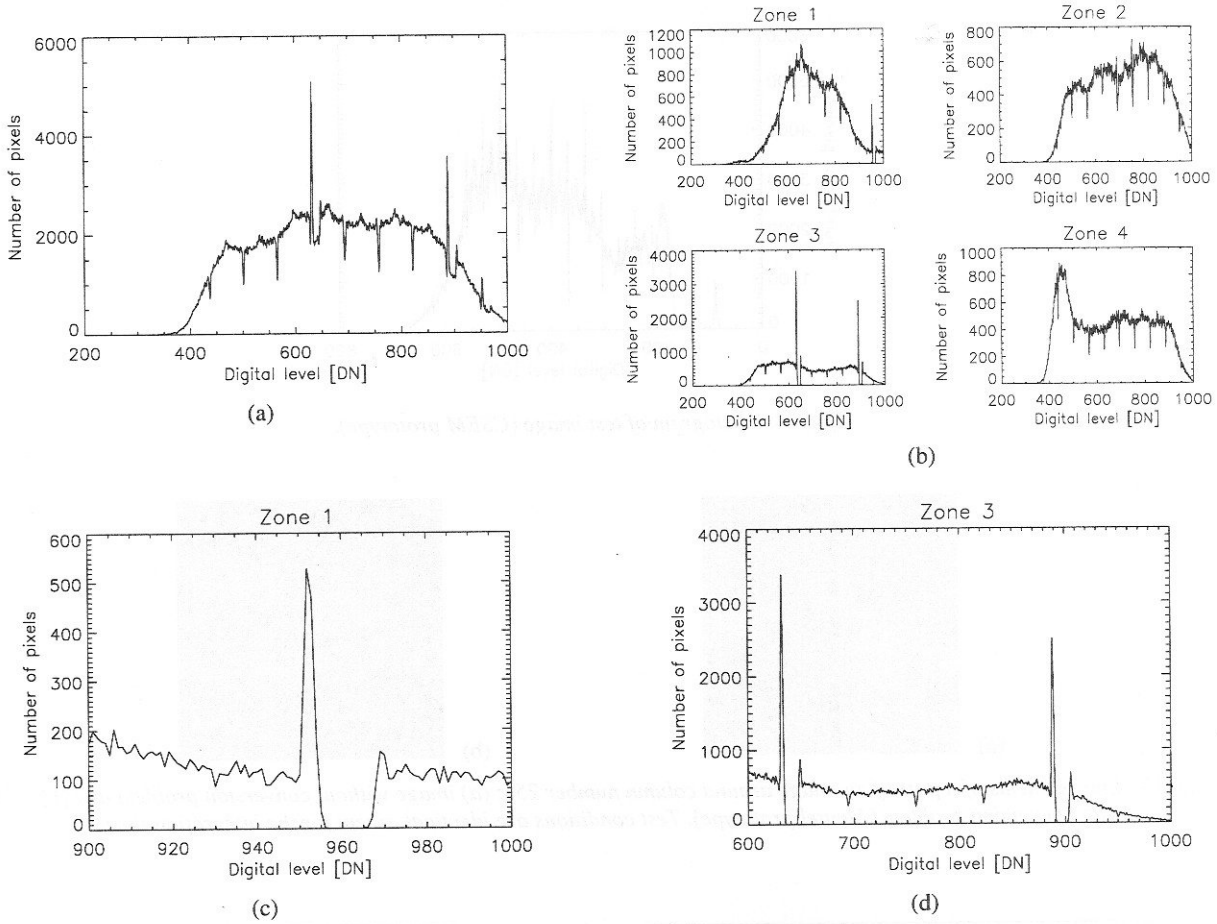

Fig. 13. *(a) Histogram of the entire test image; (b) Histograms of each zone of the array; (c) and (d) Enlargements of the histograms of zones 1 and 3 (Alcatel prototype).*

Power Consumption

The power consumption of the Alcatel prototype was measured at room temperature and at –55°C. The results show that it increases with decreasing temperature and amounts to about 30% on the 15V line. This behaviour is due to a specific increase of the CCD amplifier power consumption at low temperatures.

Analog to Digital Conversion

The performances of the electronic chain, in particular of the analog to digital conversion, were verified by projecting onto the CCD a test image whose intensity distribution covers a large part of the dynamic of the converter. For the Alcatel prototype, the histogram of this test image (Figure 13a) reveals periodic peaks separated by 64 levels, which result from the operating mode of the analog to digital converter: the 4 most significant bits are first digitised and then, in a second conversion, the 6 less significant bits. The peaks appear between the two conversions, i.e. every 64 bits. We can also notice the presence of two prominent peaks and several holes in the histogram. Figure 13b presents the histograms of each of the four zones of the array and reveals large peaks followed by holes, in the first and third zones. Enlargements of the histograms show that levels 957 to 965 are missing in the first zone (Figure 13c) while levels 636 to 645 and 892 to 902 are missing in the third zone (Figure 13d). Non-coded pixels (the holes) are shifted to the neighbouring levels, preferentially towards the lower values, thus explaining the presence of the large peaks. This problem can either be traced to a defect in the A/D converters or to a problem resulting from their integration in the 3D package. Similar periodic peaks are also present in the histogram of the CSEM images (Figure 14) but no missing codes were found.

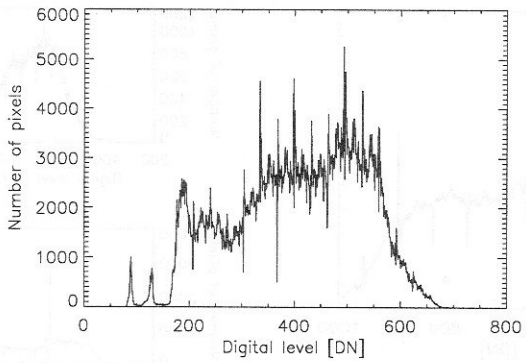

Fig. 14. *Histogram of test image (CSEM prototype).*

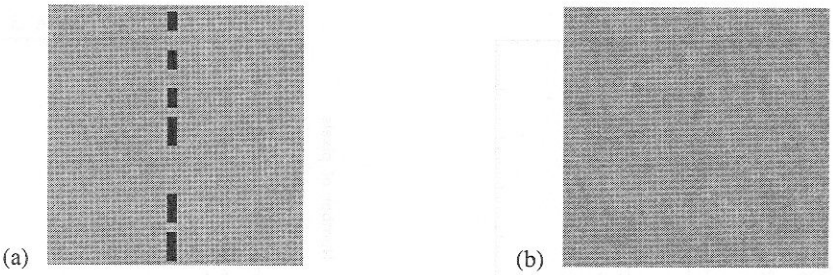

Fig. 15. *Enlargements of a part of an image around column number 256: (a) image without conversion problem and (b) image with conversion problem (Alcatel prototype). Test conditions are identical except for the integration time.*

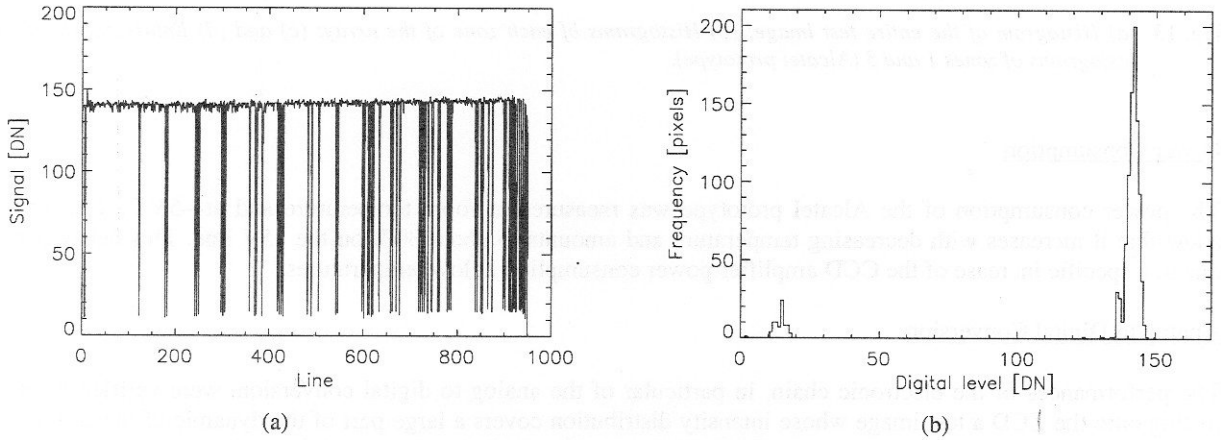

Fig. 16. *(a) Profile of the last column of the first zone for an average signal level of about 150 DN at –55°C. (b) Histogram of this column (Alcatel prototype).*

Figure 15 reveals a specific problem found while taking flat-field images in identical conditions, except for different exposure times, with the Alcatel prototype, and which affects the last column of the first zone of the array. A profile of this column shows that many pixels have an anomalous low level (Figure 16a). The histogram of this column presents two peaks separated by 128 levels (Figure 16b) proving that the 8^{th} bit of the A/D converter is malfunctioning. This problem, which persists at any temperature and at any level of illumination, should be attributed to a perturbation coming from a neighbouring logical signal. This undesired coupling probably results from the inappropriate mounting of the components on the layers stacked in the cube.

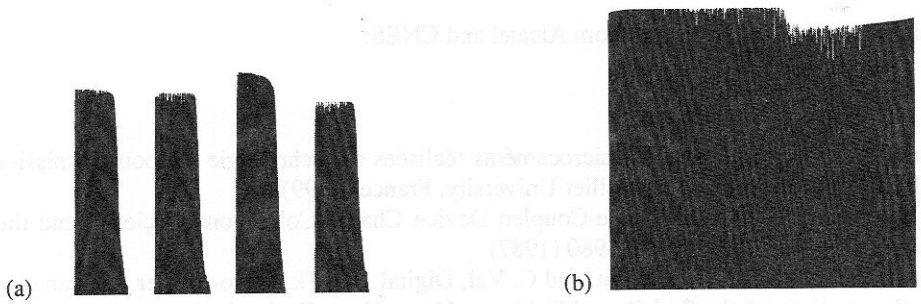

Fig. 17. *(a) Image obtained in darkness with a cleaning time of 1 second for the Alcatel prototype and (b) image obtained in darkness for the CSEM prototype.*

Memory Zone Cleaning

The Alcatel prototype contains a cleaning mode in which lines are accumulated in the output register and then readout, in order to clean the memory zone of residual charges before taking an image. To evaluate the efficiency of this cleaning mode, we took several images with different cleaning times in total darkness. Without cleaning, the images are saturated. Figure 17a shows the image obtained after a cleaning time of 1 second to be compared with Figure 17b obtained with the CSEM prototype which has no cleaning mode. In both cases, extended saturated (white) zones are present, mainly for the Alcatel prototype. They result from the charges accumulated in the memory zones which are not evacuated before image acquisition.

Operations at Very Low Temperatures

Figure 18a displays an image of a flat field taken with the Alcatel prototype at –100°C in which the fourth zone of the array gives no response. The temperature was then increased to +20°C and a functional test was performed revealing that the prototype did not function any more.

An enlargement of the top left corner of the first zone of the image reveals a blurred area and a white column (Figure 18b), suggesting a mechanical disruption. This was confirmed by a visual inspection of the CCD. In addition, a binocular inspection of the camera revealed a detachment between the cube and the titanium interface. We conclude that the mechanical design of this prototype is not capable of supporting temperatures below –90°C.

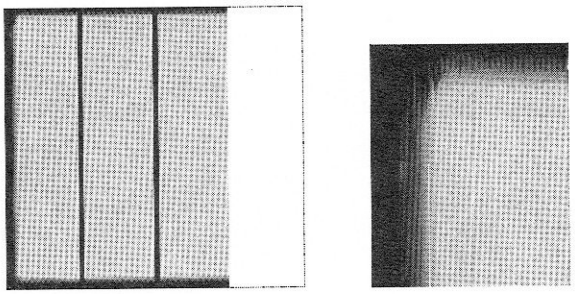

Fig. 18. *(a) Flat field image obtained with an integration time of 1500 ms at –100°C. (b) Enlargement of the top left corner of the image (Alcatel prototype).*

CONCLUSION

Our results obtained on two different prototypes reveal that the opto-electrical performances of microcameras manufactured in 3D technology are nominal and do not change in the temperature range –90°C to +20°C. However, the reduced size of the cameras leads to high internal temperature increases during image acquisitions and might be a problem when operated at temperatures above –55°C. We have also shown that care must be taken in the electrical and mechanical design of such microcameras in order to avoid functional problems and mechanical disruption at very low temperatures. Despite these problems, we can conclude that such miniature cameras, manufactured in 3D packaging technology, are suitable to deep space missions like ROSETTA.

ACKNOWLEDGEMENTS

This research was partially supported by grants from Alcatel and CNES.

REFERENCES

Beauvivre, S., Evaluation des performances de microcaméras réalisées en technologie 3D pour la mission spatiale cométaire ROSETTA, Ph.D. Thesis, Montpellier University, France (1999).

Janesick, J.R., K. Klaasen, and T. Elliott, Charge-Coupled Device Charge-Collection Efficiency and the Photon-Transfer Technique, *Opt. Eng.*, **26** (10), 972-980 (1987).

Josset, J.-L., F. Roussel, P. Plancke, G. Boucharlat, and C. Val, Digital 1k x 1k Micro-Imager for Planetary Surface Exploration, in *Proceedings of the 2nd Round Table on Micro-Nano Technologies for Space*, ESA/ESTEC (1997).

Lamy, P., J.-P. Bibring, T. Nguyen-Trong, A. Soufflot, J.-L. Boit, and K. Dohlen, The Panoramic Cameras for the Champollion and Roland Cometary Surface Science Packages, *Adv. Space Res.*, **21** (11), 1581-1588 (1998).

Larcombe, S.P., J.M. Stern, P.A. Ivey, N.L. Seed, and A.J. Shelley, A Micro-packaged Image Acquisition and Processing Module, in *Fifth International Conference on Image Processing and its Applications*, 455-459 (1995).

Val, C., and M. Leroy, The 3D-Interconnection – Applications for Mass Memories and Microprocessors, in *ISMH*, 62-68 (1991).